

# Semantic Context Matters: Improving Conditioning for Autoregressive Models

Dongyang Jin\*, Ryan Xu\*, Jianhao Zeng, Rui Lan,  
Yancheng Bai<sup>‡†</sup>, Lei Sun<sup>†</sup>, and Xiangxiang Chu  
Amap, Alibaba Group

12332451@mail.sustech.edu.cn, ryansxu.00@gmail.com, 18826077660@163.com,  
{zengjianhao.zjh, yancheng.byc, ally.sl, chuxiangxiang.cxx}@alibaba-inc.com

## Abstract

Recently, autoregressive (AR) models have shown strong potential in image generation, offering better scalability and easier integration with unified multi-modal systems compared to diffusion-based methods. However, extending AR models to general image editing remains challenging due to weak and inefficient conditioning, often leading to poor instruction adherence and visual artifacts. To address this, we propose **SCAR**, a **Semantic-Context-driven** method for **Autoregressive** models. SCAR introduces two key components: **Compressed Semantic Prefilling**, which encodes high-level semantics into a compact and efficient prefix, and **Semantic Alignment Guidance**, which aligns the last visual hidden states with target semantics during autoregressive decoding to enhance instruction fidelity. Unlike decoding-stage injection methods, SCAR builds upon the flexibility and generality of vector-quantized-based prefilling while overcoming its semantic limitations and high cost. It generalizes across both next-token and next-set AR paradigms with minimal architectural changes. SCAR achieves superior visual fidelity and semantic alignment on both instruction editing and controllable generation benchmarks, outperforming prior AR-based methods while maintaining controllability. Code will be released at <https://github.com/AMAP-ML/SCAR>.

## 1. Introduction

The advent of large-scale generative models [15, 16, 24, 36, 56] has revolutionized the field of image editing [46, 89], opening up unprecedented possibilities for creative expression and content manipulation. Within this rapidly evolving landscape, two dominant generative paradigms have emerged: diffusion [19, 53] and autoregressive (AR) models [69, 71]. Diffusion models, renowned for their powerful text-to-image synthesis capabilities, demonstrate a strong grasp of semantic concepts, allowing for flexible and di-

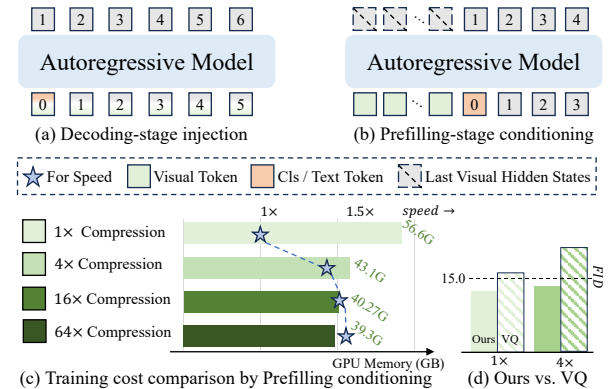


Figure 1. (a) Decoding-stage injection and (b) Prefilling-stage conditioning for condition injection. (c) Training cost under different visual token compression. 4× reduces GPU memory usage by 23.9% (from 56.6 to 43.1GB) and accelerates training by 1.42×. (d) Comparison between ours and VQ token prefilling.

verse edits based on user prompts. Concurrently, autoregressive models, owing to their excellent scaling properties and immense potential within unified multimodal generation and understanding model (UMM) architectures [35, 96], have achieved generation quality approaching that of top-tier diffusion models, establishing them as a critical and highly promising direction for future research.

However, translating this raw generative power into versatile, general image editing capabilities remains a significant challenge for AR models. Compared to diffusion-based editing methods [4, 27, 58, 89], recent AR-based approaches [32, 50] have yet to achieve the same level of semantic control and general editing scope. These works can be broadly categorized into two types based on their conditioning strategies: (1) **Decoding-stage injection** (Figure 1.a), as in *ControlAR* [32], injects condition signals into the model’s intermediate layers. It performs excellent controllable generation, but the injected strong spatial guidance disrupts the autoregressive process for general editing (see Figure 6). (2) **Prefilling-stage conditioning** (Figure 1.b), employed by works like *EditAR* [50] and most UMMs [5, 26, 81, 96], prepends visual tokens from the con-

\*Equal contribution.

†Corresponding author.

‡Project Leader.

dition image to the input sequence. However, this method introduces debilitating computational overhead: prepending vector-quantized (VQ) tokens of the condition image can double the sequence length, increasing the computational cost, as shown in Figure 1.c. Moreover, VQ tokens are widely recognized as sparse-semantic [6, 40, 80], lacking the high-level representation needed for complex edits.

In this work, we revisit the prefilling conditioning paradigm from a semantic perspective and argue that it offers a powerful route toward general image editing and is also compatible with various AR paradigms. We identify the prefilling bottleneck as their reliance on inefficient and VQ-based prefixes with shallow semantics. Our approach introduces two key innovations.

First, we propose **Compressed Semantic Prefilling**, which replaces the inefficient VQ token prefix with compact, rich-semantic vision features extracted from the source image via a frozen vision foundation model (VFM) [10, 52, 61]. We introduce a learnable semantic compression module that drastically reduces the prefilling sequence length (e.g.,  $4\times$  compression from 1024 to 256 tokens) while preserving essential high-level semantics for editing. This significantly enhances computational efficiency and provides the model with a compact semantic understanding of the source content before generation, as shown in Figure 1.d. Notably, our semantic prefix remains robust even when compressed, while VQ token prefix suffers sharp performance drops under similar settings.

Second, to bridge the gap between sparse textual instructions and the desired dense visual guidance, we introduce a novel **Semantic Alignment Guidance**. Instead of relying solely on the sparse text condition, we use the visual features of the target edited image from the VFM as a dense semantic guide. Unlike the prior method [50] that distills supervision onto output VQ tokens, we apply an auxiliary constraint objective that aligns the autoregressive model’s last visual hidden states with the target’s semantic representation, providing a formulation more consistent with the causal decoding process. This provides a dense, in-context learning signal that steers the model’s internal reasoning toward the edit target.

Our contributions can be summarized as follows:

- We present a **Semantic-Context-driven Autoregressive method (SCAR)** for general image editing, designed to integrate with most autoregressive models seamlessly.
- We design **Compressed Semantic Prefilling**, an efficient visual token compression mechanism to produce compact semantic features for conditioning autoregressive models, overcoming the limitations of VQ-based prefilling.
- We introduce **Semantic Alignment Guidance**, providing dense, progressive, in-context semantic guidance to the autoregressive process, enabling complex and semantically-accurate edits.

- We demonstrate state-of-the-art performance on challenging instruction editing and controllable generation benchmarks, proving SCAR is more effective, efficient, and semantically-aware than existing AR editing frameworks.

## 2. Related Work

### 2.1. Image Generation

Two dominant paradigms have emerged in image generation: diffusion models and AR models. Diffusion models synthesize images by iteratively denoising Gaussian noise, with DDPM [20] marking a major breakthrough. Subsequent work improves generation quality and efficiency [51, 59, 64, 75, 76, 91] through advances in sampling strategies and latent-space modeling. They have become the backbone of text-to-image and text-to-video generation [7, 24, 41, 65, 67, 77, 88, 92], typically using U-Net for denoising and CLIP [61, 78] or T5 [62] for text conditioning via cross-attention. Recent models like DiT [53] replace U-Net with Transformer backbones, achieving strong performance. Despite their success, diffusion models remain computationally expensive, motivating exploration of more efficient alternatives such as autoregressive approaches.

In contrast, autoregressive (AR) models formulate image synthesis as a sequence modeling problem, predicting visual tokens step by step. Early works [73] focused on pixel-level generation. Building on the success of large language models [1, 72], recent approaches adopt discrete quantizers such as VQ-VAE [74] and VQ-GAN [11] to convert image patches into token indices, enabling next-token prediction over visual sequences. Recent advances have expanded this paradigm in two directions: (1) conventional next-token AR models [39, 43, 45], such as LlamaGen [69] and AiM [25], leverage large-scale transformer backbones for high-quality image synthesis; and (2) Visual Autoregressive Modeling (VAR), which reformulates generation as next-set prediction rather than raster-scan token prediction, offering improved scalability and global coherence [15, 42, 70, 71, 96]. Overall, AR-based approaches have achieved image quality comparable to diffusion models while being more efficient in sampling and deployment.

### 2.2. General Image Editing

General Image editing, including controllable and instruction editing, is a key focus in generative modeling, guided by external signals (e.g., text, edge maps, reference images). While early approaches incorporated class labels or attributes in GANs [47, 68] and VAEs [22, 87], recent diffusion-based methods [49, 58, 89] achieve fine-grained control via cross-attention or adapter modules. Building on this, text-guided instruction editing methods [4, 17, 46] further extend controllable generation to image manipulation. However, these approaches often involve costly inversion,

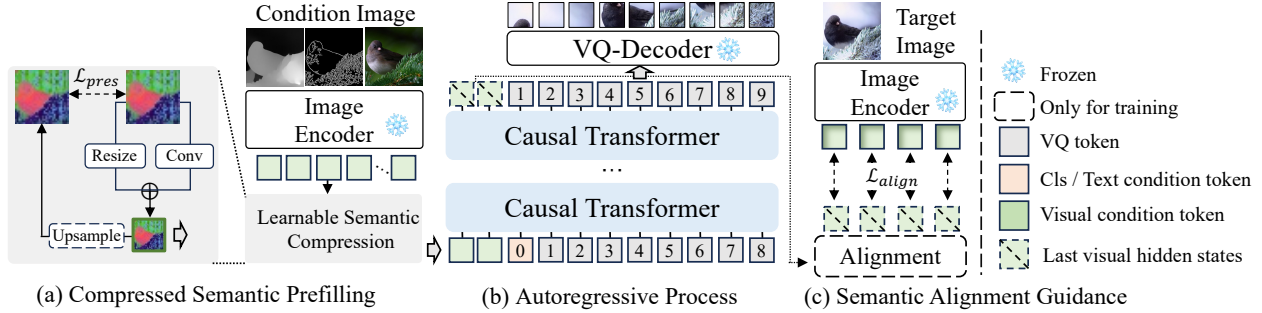


Figure 2. Overview of our proposed **SCAR**, a prefilling-based method for autoregressive image editing. SCAR is composed of (a) **Compressed Semantic Prefilling** (see Section 3.2 for details) and (c) **Semantic Alignment Guidance** (see Section 3.3 for details), jointly enabling semantically guided generation. The framework is general and compatible with both *next-token* and *next-set* AR paradigms.

require modality-specific tuning, or suffer from limited generalization across tasks and conditions.

In contrast, image editing with autoregressive (AR) models, including next-token and next-set paradigms, remains relatively underexplored. Recent AR-based methods can be broadly categorized by the stage at which control signals are injected: **Decoding-stage injection** [32, 83, 85] introduces control signals dynamically during generation, typically via cross-attention or feature modulation. These approaches offer strong controllability for pixel-level generation, but their complex architectural modifications often limit generalization to instruction-driven editing. **Prefilling-stage conditioning** [30, 35, 50, 60, 81, 96] prepends visual tokens from the source image to the input sequence, enabling conditioning before generation. This paradigm is adopted by EditAR [50] and VARSR [60]. While simple and model-agnostic, such strategies significantly increase sequence length and attention cost, limiting the model’s capacity for precise and instruction-aware editing. Furthermore, directly concatenating raw control tokens (e.g., in ControlVAR [30]) may disrupt the pretrained generation behavior of the AR backbone. The reliance on semantically sparse VQ tokens further limits the effectiveness of prefilling-based approaches [6, 40, 80]. In this paper, we adopt prefilling-stage conditioning and propose a compact semantic method for better guidance. Our method applies to both next-token and next-set AR models with minimal architectural changes.

### 3. SCAR

In this section, we present SCAR, an efficient conditioning strategy for general AR models, as shown in Figure 2. We first revisit the image generation with general AR (Section 3.1). Next, we introduce Compressed Semantic Prefilling (Section 3.2) for the vision prefix. Finally, we improve sparse instruction guidance via Semantic Alignment Guidance in Section 3.3.

#### 3.1. Preliminary

Autoregressive (AR) models extend the success of large language models [1, 72] to image generation and have become a popular approach in vision. These models convert images into discrete tokens using vector quantization (e.g., VQVAE [74]) and generate outputs by predicting tokens conditioned on preceding context. Recent AR approaches can be broadly categorized into two types: *next-token prediction*, which autoregressively generates individual tokens along a raster-scan sequence [25, 69], and *next-set prediction*, which generates a set of tokens following specialized principles (e.g., VAR [71] predicts next-scale tokens in a coarse-to-fine manner). Despite the difference in basic token units (single token vs. a set of tokens), both follow a unified autoregressive formulation:

$$p(\mathbf{z}) = \prod_{i=1}^N p(z_i | z_{<i}, c), \quad (1)$$

where  $\mathbf{z} = \{z_1, z_2, \dots, z_N\}$  denotes the sequence of discrete visual token units, and  $c$  represents the conditioning input, such as class labels, text prompts, or control features. The model is trained by minimizing the negative log-likelihood of the token sequence using a cross-entropy loss:

$$\mathcal{L}_{CE} = \mathbb{E}_{z_i \sim p(z_i)} [-\log p_{\theta}(z_i | z_{<i}, c)]. \quad (2)$$

This general formulation provides a flexible training objective that accommodates a wide range of AR paradigms for generation and editing tasks.

#### 3.2. Compressed Semantic Prefilling

Our primary objective in the prefilling stage is to establish a conditioning prefix that is simultaneously computationally efficient (via short sequence length) and with rich semantics. To this end, we leverage powerful pre-trained Vision Foundation Models (VFM)  $\mathcal{E}(\cdot)$  to encode the source condition image, and adopt DINOv2 [52] in practice. However, this choice introduces a direct conflict with our goal of efficiency. For a standard  $512 \times 512$  input, they produce a

sequence of 1024 tokens. As illustrated in Figure 1, this verbose prefix without compression leads to severe computational and memory overhead. To retain the rich semantics of VFMs while achieving a compact prefix, we propose a novel learnable token compression module.

**Learnable Semantic Compression.** Directly using the semantic feature token  $\mathbf{F}_s = \mathcal{E}(\mathbf{I}_s)$  of the source condition image  $\mathbf{I}_s$  as a prefix is still inefficient, as  $\mathbf{F}_s \in \mathbb{R}^{h \times w \times d}$  can contain over 1024 tokens (e.g.,  $h \times w = 32 \times 32$ ), where  $d$  is the feature dimension. To address this, we introduce a learnable semantic compressive module  $\mathcal{P}_k(\cdot)$ , which compresses the vision features by a factor of  $k$  while preserving high-level semantics. Specifically, it compresses the source feature map through a spatial downsampling  $\mathcal{R}_k(\cdot)$  and a paralleled stride convolution downsampling  $\mathcal{C}_k(\cdot)$ :

$$\mathbf{F}_c = \mathcal{P}_k(\mathbf{F}_s) = \mathcal{C}_k(\mathbf{F}_s) + \mathcal{R}_k(\mathbf{F}_s), \quad (3)$$

where  $\mathbf{F}_c \in \mathbb{R}^{\frac{h}{k} \times \frac{w}{k} \times d}$  is the compressed semantic feature.

To ensure  $\mathcal{P}_k(\cdot)$  learn to preserve critical semantic information during this compression, we train it with a lightweight upsampling module  $\mathcal{U}_k$  implemented as a pixel shuffle operation [44, 66] with a **semantic preservation loss**:

$$\mathcal{L}_{pres} = \|\mathbf{F}_s - \mathcal{U}_k(\mathbf{F}_c)\|_2^2. \quad (4)$$

This loss, computed in the vision feature space, trains  $\mathcal{P}_k(\cdot)$  to retain enough information necessary for semantic reconstruction, discarding redundant details. At inference,  $\mathcal{U}_k(\cdot)$  is discarded.

**Input Sequence Formulation.** The final input sequence  $\mathbf{S}$  fed to the Causal Transformer  $\mathcal{G}_\theta$  is the concatenation of the compressed source condition semantic sequence  $\mathbf{P}_s$ , the target text embedding  $\mathbf{T}_t$ , and the VQ sequence of the target edited image  $\mathbf{Z}_t$ :

$$\mathbf{S} = [\mathbf{P}_s; \mathbf{T}_t; \mathbf{Z}_t], \quad (5)$$

where  $\mathbf{P}_s \in \mathbb{R}^{L_c \times d}$  is the flattened sequence obtained from the compressed feature map  $\mathbf{F}_c$ , and  $L_c = \frac{h \times w}{k^2}$  denotes the reduced token length. We achieve a  $k^2 \times$  **compression** compared to directly prefilling.

We also change the attention mask. Specifically,  $\mathbf{P}_s$  and  $\mathbf{T}_t$  attend to each other bidirectionally, allowing for deep interaction of visual and text semantic information. The quantized tokens  $\mathbf{Z}_t$  attend causally to the prefix  $[\mathbf{P}_s; \mathbf{T}_t]$  and all preceding VQ tokens, maintaining the autoregressive property for generation.

### 3.3. Semantic Alignment Guidance

A fundamental challenge in instruction-guided editing is the semantic gap. The text prompt provides only sparse, high-level guidance, which is often insufficient to steer the generation of thousands of dense, low-level VQ tokens  $\mathbf{Z}_t$ . The standard autoregressive loss  $\mathcal{L}_{CE}$  (in Equation (5)) provides

supervision on  $\mathbf{Z}_t$ , but it does not explicitly teach the model how to use the context  $[\mathbf{P}_s; \mathbf{T}_t]$  to achieve the desired edit. To bridge this gap, we introduce the Semantic Alignment Guidance. The core innovation is to provide a dense, in-context learning signal that teaches the model to understand the target semantics  $\mathbf{P}_t$  via source semantics  $\mathbf{P}_s$  before it even generates the first VQ token.

Specifically, we compute the dense semantic representation of the target image  $\mathbf{I}_t$ . We use the same frozen, pre-trained  $\mathcal{E}(\cdot)$  and our same learnable compressor  $\mathcal{P}_k(\cdot)$  to ensure the compressed semantic source and target representations lie in the same space:

$$\mathbf{P}_t = \mathcal{P}_k(\mathcal{E}(\mathbf{I}_t)), \quad (6)$$

where  $\mathbf{P}_t \in \mathbb{R}^{L_c \times d}$  serves as our ground-truth semantic target. In the training phase, we feed the input sequenced  $\mathbf{S}$  through the causal transformer  $\mathcal{G}_\theta$  and extract the last output hidden states  $\mathbf{H}_s$  corresponding to the source semantic tokens  $\mathbf{P}_s$ :

$$\mathbf{H} = \mathcal{G}_\theta(\mathbf{S}), \quad \mathbf{H}_s = \mathbf{H}[1 : L_c, :], \quad (7)$$

where  $\mathbf{H}_s$  represents the autoregressive model’s internal reasoning of the source image after being modulated by the edit instruction. Our semantic alignment guidance then forces this internal understanding  $\mathbf{H}_s$  to align with the target semantic representation  $\mathbf{P}_t$  via a  $\ell_2$  constraint:

$$\mathcal{L}_{align} = \|\mathbf{H}_s - \mathbf{P}_t\|_2^2. \quad (8)$$

This objective serves as a dense and semantically grounded guidance signal, encouraging the model to align its internal representation of the source condition toward the desired target semantics, providing a rich in-context prior that significantly eases the subsequent prediction of accurate VQ tokens  $\mathbf{Z}_t$ . Besides, this alignment operates within a unified feature space, ensuring semantic consistency and stable optimization across both source and target representations.

## 4. Experiments

### 4.1. Experimental Setup

**Dataset.** We evaluate our method on controllable generation, covering class-to-image (C2I), text-to-image (T2I), and instruction editing tasks. For C2I controllable generation, models are trained on ImageNet-256 [9] with five types of control conditions: Canny, Depth, Normal, HED, and Sketch. For T2I controllable generation, we use the MultiGen-20M [58] for training, considering Depth, Canny, HED, and Lineart as control conditions. For instruction editing, training is conducted on SEED-Edit-Unsplash [13].

**Training Details.** (1) We use DINOv2-B [52] as the image encoder due to its strong visual representations and scalability. (2) For C2I controllable generation at a resolution of

Table 1. Quantitative results of C2I controllable generation on ImageNet [9]. Values marked with ~ are estimated from histograms in the corresponding paper. Cells highlighted with   and   denote the best performance under the **next-set** and **next-token** autoregressive settings, respectively. **SCAR-Uni** denotes a unified model trained jointly across all conditions, rather than SCAR for each condition.

Type	Method	Model	Canny		Depth		Normal		HED		Sketch	
			FID↓	F1-Score↑	FID↓	RMSE↓	FID↓	RMSE↓	FID↓	SSIM↑	FID↓	F1-Score↑
Diff.	T2IAdapter [48]	SD1.5	~10.2	-	~9.9	-	~9.5	-	~9.3	-	~16.2	-
	ControlNet [90]	SD1.5	~11.6	-	~9.2	-	~8.9	-	~8.6	-	~15.3	-
AR	ControlAR [32]	AiM-L	9.66	30.36	7.39	35.01	-	-	-	-	-	-
		LlamaGen-B	10.64	34.15	6.67	32.41	-	-	-	-	-	-
		LlamaGen-L	7.69	34.91	4.19	31.11	-	-	-	-	-	-
	ControlVAR [30]	VAR-d16	~16.2	-	~13.8	-	~14.2	-	-	-	-	-
		VAR-d20	~13.0	-	~13.4	-	~12.8	-	-	-	-	-
		VAR-d30	7.85	-	6.50	-	6.20	-	-	-	-	-
	CAR [85]	VAR-d16	~12.8	-	~10.8	-	~11.0	-	~9.8	-	~13.2	-
		VAR-d20	~10.2	-	~8.0	-	~8.8	-	~7.2	-	~11.2	-
		VAR-d30	8.30	-	6.90	-	6.60	-	5.60	-	10.20	-
	SCAR-Uni (Ours)	VAR-d16	2.77	29.41	4.29	35.61	4.14	28.51	2.40	75.29	4.59	76.88
		VAR-d20	2.22	29.61	3.27	35.08	3.16	27.73	1.98	75.67	3.37	77.06
		LlamaGen-B	4.92	30.69	5.04	36.60	4.82	28.48	4.18	75.24	5.86	76.41
		LlamaGen-L	2.54	31.27	2.77	34.35	2.51	27.73	2.39	77.08	3.02	77.51
	SCAR (Ours)	VAR-d12	2.88	29.82	3.46	34.61	3.60	27.74	2.11	77.81	4.40	77.17
		VAR-d16	2.10	30.95	3.54	33.33	3.18	26.88	1.81	78.61	3.83	77.83
		VAR-d20	1.97	31.27	3.29	33.32	2.96	26.73	1.51	79.72	3.39	77.74
		LlamaGen-B	5.32	31.57	4.20	34.36	4.06	26.77	3.89	78.28	4.58	77.57
		LlamaGen-L	2.69	31.82	2.69	32.82	2.50	26.05	2.67	79.29	3.04	78.30

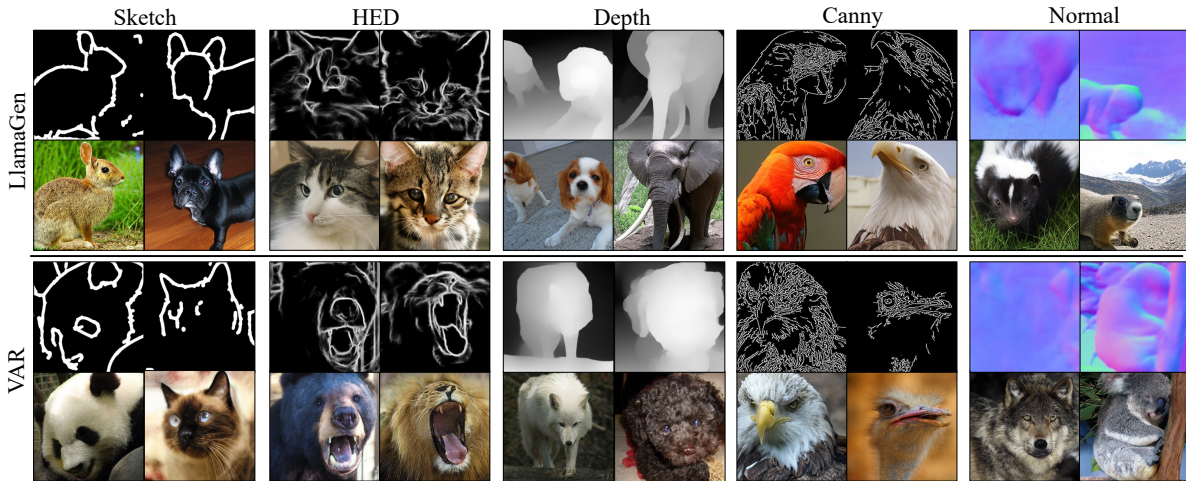


Figure 3. Visualization of C2I controllable generation. Our SCAR demonstrates results respectively based on VAR [71] and LlamaGen [69].

$256 \times 256$ , we adopt two types of models: next-set VAR [71] and next-token LlamaGen [69]. In this task, SCAR-Uni denotes a variant trained with uniformly sampled control types, supporting any control input at inference. (3) We use LlamaGen-XL with a T5 encoder [62] at  $512 \times 512$  for both T2I controllable generation and instruction editing, using captions and editing instructions as text inputs, respectively. (4) We train VAR for 10 epochs and LlamaGen for 20 epochs on C2I controllable generation, 4 epochs on T2I controllable generation, and 2 epochs on instruction editing. (5) All models are trained on 8 NVIDIA H20 GPUs.

**Evaluation and Metrics.** For controllable generation, we evaluate models based on two main aspects: conditional

consistency and image generation quality. Conditional consistency is measured by comparing the input condition image with the condition image extracted from the generated output. We use F1-Score for Canny and Sketch, Root Mean Square Error (RMSE) for Normal and Depth, and Structural Similarity Index Measure (SSIM) for HED and Lineart. Image generation quality is assessed using Fréchet Inception Distance (FID) [18]. Class-to-image (C2I) evaluations are conducted on the full 50K validation set of ImageNet-256, while text-to-image (T2I) evaluations are performed on the official 5K validation set of MultiGen-20M [58].

For instruction editing, we adopt the PIE-Bench [21], containing 700 samples covering 10 editing types. SCAR

Table 2. Image generation quality and conditional consistency of T2I controllable generation on MultiGen-20M [58]. Our SCAR is based on LlamaGen-XL. **Bold** indicates the best result and underline indicates the second best. The results are conducted on  $512 \times 512$  resolution.

Type	Method	Depth		HED		Canny		Lineart	
		FID↓	RMSE↓	FID↓	SSIM↑	FID↓	F1-Score↑	FID↓	SSIM↑
Diff.	GLIGEN [31]	18.36	38.83	-	-	18.89	26.94	-	-
	T2I-Adapter [48]	22.52	48.40	-	-	15.96	23.65	-	-
	ControlNet [90]	17.76	35.90	15.41	76.21	14.73	34.65	17.44	70.54
	Uni-ControlNet [93]	20.27	40.65	17.08	69.10	17.14	27.32	-	-
	UniControl [57]	18.66	39.18	15.99	79.69	19.94	30.82	-	-
	ControlNet++ [28]	16.66	<b>28.32</b>	15.01	80.97	18.23	<u>37.04</u>	13.88	<b>83.99</b>
AR	ControlAR [32]	<u>14.61</u>	29.01	<u>10.53</u>	<b>85.63</b>	17.51	<b>37.08</b>	<u>12.41</u>	<u>79.22</u>
	EditAR [50]	15.97	34.93	-	-	13.91	-	-	-
	SCAR (Ours)	<b>13.77</b>	<u>28.89</u>	<b>8.41</b>	<u>83.09</u>	<b>10.82</b>	32.46	<b>8.91</b>	73.52

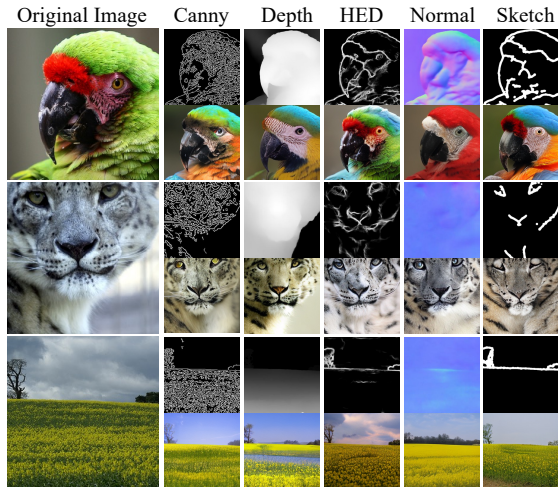


Figure 4. Visualization of multi-condition controllable SCAR-Uni (based on LlamaGen) under varying control conditions.

takes the source image and editing instructions as input to predict the target image, and follows the evaluation protocol in [21]. Evaluation metrics cover three aspects: structure consistency, background preservation, and CLIP-based image-text alignment.

## 4.2. Controllable Generation Results

**C2I Controllable Generation.** We evaluate the C2I controllable generation performance of our SCAR and its unified multi-condition variant SCAR-Uni on ImageNet [9]. As shown in Table 1, we assess both conditional consistency and image generation quality under two autoregressive paradigms: next-token-based LlamaGen and next-set-based VAR. Compared with existing C2I controllable generation methods, including diffusion-based methods [48, 90], next-token AR methods [32], and next-set AR methods [30, 85], SCAR achieves significantly better image quality (e.g., FID **1.97** vs. 7.69 on Canny), while maintaining competitive control accuracy compared to models that apply decoding-stage injection. SCAR is validated under both next-token and next-set paradigms, demonstrating the effectiveness and

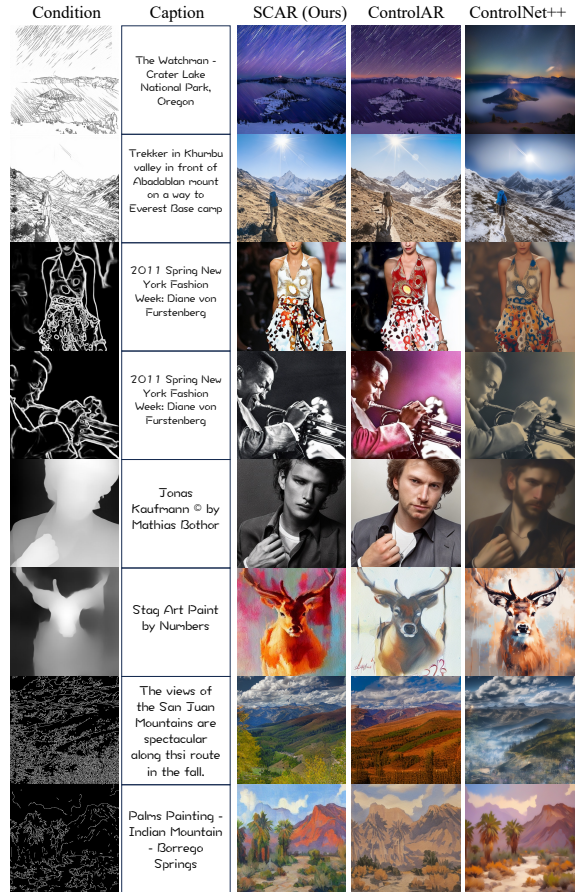


Figure 5. Visualization of T2I controllable generation. Our SCAR generates images with significantly higher visual quality.

generalizability. Figure 3 and Figure 4 further illustrate this, showing visual results of SCAR across different autoregressive paradigms, and SCAR-Uni under a unified multi-condition setting.

**T2I Controllable Generation.** We adopt LlamaGen-XL as AR model for SCAR in T2I controllable generation. Table 2 reports generation quality (FID) and controllability results across four control conditions on MultiGen-

Table 3. Quantitative comparison between our SCAR and other methods on PIE-Bench [21]. Metrics include structure consistency, background preservation, and CLIP-based image-text alignment. ControlAR\* is a retrained variant of ControlAR for editing.

Type	Method	Model	Structure	Background Preservation				CLIP Similarity	
			Distance↓	PSNR↑	LPIPS↓	MSE↓	SSIM↑	Whole↑	Edited↑
Dif.	InstructPix2Pix [4]	SD1.5	107.43	16.69	271.33	392.22	68.39	23.49	22.20
	InstructDiffusion [14]	SD1.5	74.21	20.88	142.35	353.45	76.70	24.06	21.57
	MGIE [12]	SD1.5	67.41	21.20	142.25	295.11	<b>77.52</b>	24.28	21.79
	SEED-X-Edit [13]	SDXL	61.69	18.80	173.63	209.05	75.13	<b>25.51</b>	<u>21.87</u>
AR	ControlAR* [32]	LlamaGen	116.99	14.63	289.34	590.63	63.03	23.12	21.43
	EditAR [50]	LlamaGen	<u>39.43</u>	<u>21.32</u>	<u>117.15</u>	<u>130.27</u>	75.13	24.87	<u>21.87</u>
	SCAR (Ours)	LlamaGen	<b>30.98</b>	<b>22.59</b>	<b>105.09</b>	<b>83.47</b>	<u>76.73</u>	<u>25.08</u>	<b>21.88</b>

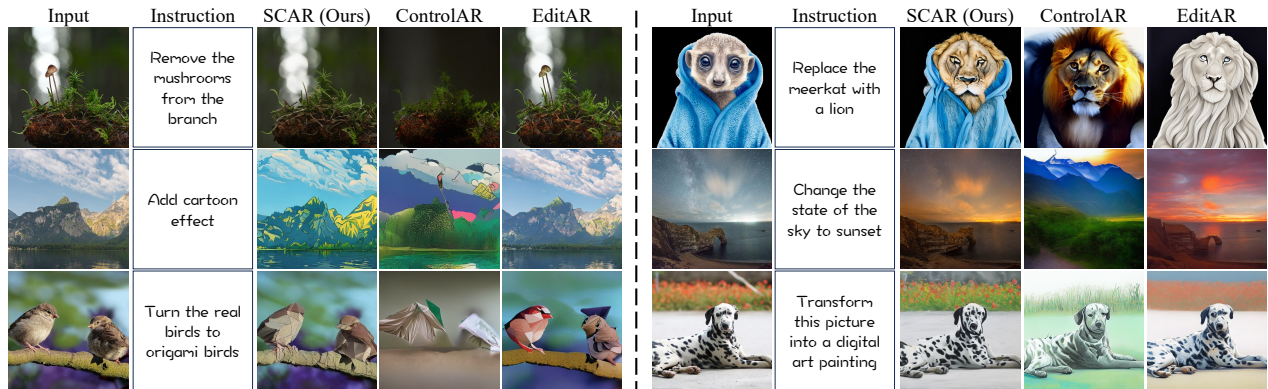


Figure 6. Qualitative results of instruction editing. Compared with other AR-based methods (ControlAR [32], EditAR [50]), SCAR can follow instructions more closely and preserve the original image content better. *Note*: more visualizations can be found in the **Appendix**.

20M [58]. Alongside representative diffusion-based methods [28, 31, 49, 58, 90, 94], we compare SCAR with recent AR-based methods, including EditAR [50] and ControlAR [32]. SCAR consistently outperforms all competing methods in FID across all conditions, achieving notably lower scores (e.g., HED: **8.41** vs. 10.53; Depth: **13.77** vs. 14.61; **Our SCAR** vs. ControlAR). While the decoding-stage injection method ControlAR achieves strong alignment, SCAR still delivers highly competitive consistency across HED, Depth, and others. Notably, under the same backbone, SCAR achieves a better balance between control accuracy and visual fidelity compared to prior methods. Figure 5 shows qualitative comparisons, where SCAR generates more natural and visually appealing results while maintaining comparable controllability.

### 4.3. Instruction Editing Results

**Quantitative Results.** Table 3 presents quantitative results on PIE-Bench [21], evaluating structure preservation, background reconstruction, and image-text alignment. Under the same backbone architecture (LlamaGen-XL), prefilling-based methods (SCAR and EditAR) substantially outperform decoding-stage injection (ControlAR). This indicates decoding-stage injection is suboptimal for instruction editing, as its strong spatial guidance tends to disrupt the autoregressive editing. SCAR achieves the best results on

most metrics, reducing structure distance by 21.4%, LPIPS by 10.3%, and MSE by 35.9%, while improving PSNR by 1.27 dB and boosting regional CLIP similarity. These gains stem from SCAR’s compressed semantic prefilling, which replaces VQ tokens with DINO features that better capture structural and semantic cues. Furthermore, Semantic Alignment Guidance further enhances instruction-result consistency.

**Qualitative Results.** As shown in Figure 6, we qualitatively compare our SCAR with AR-based methods [32, 50]. SCAR consistently follows instructions while better preserving untouched regions, avoiding unnecessary over-editing. Compared to ControlAR and EditAR, it handles fine-grained, structurally complex edits with greater precision, producing clearer boundaries and more natural textures. These results highlight SCAR’s advantages in semantic alignment, structural consistency, and visual quality. More visualizations can be found in the Appendix

### 4.4. Ablation Study

**Compression Strategies.** We compare different feature compression strategies with a  $4\times$  compression (from 1024 to 256 tokens) in Table 4. Experimental results demonstrate that our proposed Learnable Semantic Compression strategy preserves more informative features and fine details during token compression. The semantic preservation

Table 4. Ablation on different compression strategies. All models are trained for 1 epoch (including Table 5 and Table 6).

MultiGen-20M	Strategy	HED		Depth	
		FID↓	SSIM↑	FID↓	RMSE↓
	Resize	10.07	80.15	15.78	34.20
	PixelUnshuffle	<u>9.82</u>	<u>81.65</u>	15.48	34.27
	Ours	9.89	81.47	<u>15.21</u>	<b>33.90</b>
	Ours + w/ $\mathcal{L}_{pres}$	<b>9.43</b>	<b>81.76</b>	<b>14.70</b>	<u>33.95</u>

Table 5. Ablation on different compression ratios.

MultiGen-20M	Compression Ratio $k^2$ for Eq. (3)	HED		Depth	
		FID↓	SSIM↑	FID↓	RMSE↓
	1×	<b>9.29</b>	<b>81.95</b>	<b>14.61</b>	<u>34.09</u>
	4×	9.43	81.76	14.70	<b>33.95</b>
	16×	10.74	79.66	16.10	34.92

Table 6. Comparison of Image Encoders  $\mathcal{E}$  on MultiGen-20M.

Idx	Image Encoder $\mathcal{E}$	Para. of $\mathcal{E}$	HED		Depth	
			FID↓	SSIM↑	FID↓	RMSE↓
(a)	DINOv2-S	22.1M	10.25	81.19	<u>15.26</u>	<u>34.14</u>
(b)	ViT-S	21.8M	12.37	72.01	17.56	36.74
(c)	ViT-B	86.4M	11.87	77.45	16.86	36.39
(d)	SAM-B	89.6M	<u>10.20</u>	<u>81.58</u>	15.57	34.94
(e)	CLIP-B	149.6M	13.78	55.43	18.35	38.10
(f)	DINOv2-B	86.6M	<b>9.43</b>	<b>81.76</b>	<b>14.70</b>	<b>33.95</b>

loss in Equation (4) is introduced during training to guide the compression module to retain essential information for semantic recovery while discarding low-level noise and redundant details, which further enhances generation quality.

**Compression Ratio.** After adopting Learnable Semantic Compression, we further study the impact of different compression ratios. As shown in Table 5, 4× achieves comparable quality and consistency to the non-compressed setting (1×), while significantly outperforming 16×. This indicates that 4× compression effectively reduces the input tokens while preserving performance. Moreover, as shown in Figure 1, its generation speed is close to 16×, offering a good trade-off between efficiency and quality. We thus adopt 4× as the default setting.

**Ablations on Image Encoder  $\mathcal{E}$ .** In Table 6, we conduct experiments using different image encoders towards different controls on MultiGen-20M [58], including HED and Depth. Firstly, unlike previous approaches [32, 85], Our methods adopt frozen image encoders [10, 23, 52, 61] to preserve the robust features obtained from large-scale pre-training. As shown in Table 6 (a) to (c), DINOv2 [52] outperforms other pretrained vision models such as ViT [10], CLIP [61], and SAM [23]. Furthermore, comparing (b), (c), (a), and (f) indicates that increasing the scale of the image encoder significantly boosts performance. Therefore, we choose DINOv2-B as the final image encoder.

**Ablations on Semantic Alignment Guidance.** As shown in Figure 7, we perform ablation studies on the proposed

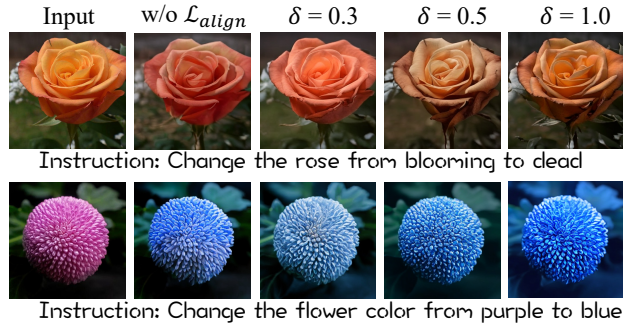


Figure 7. Ablation studies on Semantic Alignment Guidance  $\mathcal{L}_{align}$  in Equation (8).

Semantic Alignment Guidance to assess its effectiveness in improving instruction adherence. As shown in Figure 7, we conduct ablation studies on Semantic Alignment Guidance to assess its effect on instruction fidelity. Without the alignment loss  $\mathcal{L}_{align}$ , the model sometimes fails to follow the editing instructions, leading to semantic mismatches. Introducing the Semantic Alignment Guidance significantly enhances the model’s ability to follow instructions, with outputs better aligned to the target semantics. As the alignment weight  $\delta$  increases, instruction fidelity improves; however, overly strong guidance (e.g.,  $\delta = 1.0$ ) may cause artifacts such as structural distortion (row 1) or color spillover (row 2). We find that setting  $\delta = 0.5$  offers the best trade-off between semantic consistency and visual quality, highlighting the effectiveness of our alignment strategy.

## 5. Conclusion and Future Work

**Conclusion.** In this work, we present SCAR, a prefilling-based conditioning method adaptable to both *next-token* and *next-set* autoregressive models. To overcome the limitations of existing AR-based editing methods, SCAR introduces two key innovations: **Compressed Semantic Prefilling**, which injects compact and semantically-rich DINO features for improving conditioning; and **Semantic Alignment Guidance**, which provides dense supervision by aligning intermediate hidden states with target image semantics. These designs significantly improve both editability and controllability across diverse tasks. Our SCAR demonstrates superior performance in controllable generation and instruction editing, while remaining compatible with modern unified AR architectures. We hope our work inspires further research into semantic and efficient conditioning strategies for autoregressive models.

**Future Work.** (1) Scaling SCAR to larger parameter sizes may enhance performance further, following the scaling law of autoregressive models to improve semantic understanding and controllability. (2) Extending SCAR beyond general image editing to broader generative tasks, such as unified multimodal models and video editing.

## References

- [1] Josh Achiam, Steven Adler, Sandhini Agarwal, Lama Ahmad, Ilge Akkaya, Florencia Leoni Aleman, Diogo Almeida, Janko Altenschmidt, Sam Altman, Shyamal Anadkat, et al. Gpt-4 technical report. *arXiv preprint arXiv:2303.08774*, 2023. 2, 3
- [2] Ruichuan An, Sihan Yang, Ming Lu, Renrui Zhang, Kai Zeng, Yulin Luo, Jiajun Cao, Hao Liang, Ying Chen, Qi She, et al. Mc-llava: Multi-concept personalized vision-language model. *arXiv preprint arXiv:2411.11706*, 2024. 13
- [3] Ruichuan An, Sihan Yang, Renrui Zhang, Zijun Shen, Ming Lu, Gaole Dai, Hao Liang, Ziyu Guo, Shilin Yan, Yulin Luo, et al. Unictokens: Boosting personalized understanding and generation via unified concept tokens. *arXiv preprint arXiv:2505.14671*, 2025. 13
- [4] Tim Brooks, Aleksander Holynski, and Alexei A Efros. Instructpix2pix: Learning to follow image editing instructions. In *Proceedings of the IEEE/CVF conference on computer vision and pattern recognition*, pages 18392–18402, 2023. 1, 2, 7
- [5] Siyu Cao, Hangting Chen, Peng Chen, Yiji Cheng, Yutao Cui, Xincheng Deng, Ying Dong, Kipper Gong, Tianpeng Gu, Xiuse Gu, et al. Hunyuanimage 3.0 technical report. *arXiv preprint arXiv:2509.23951*, 2025. 1
- [6] Jiu Hai Chen, Zhiyang Xu, Xichen Pan, Yushi Hu, Can Qin, Tom Goldstein, Lifu Huang, Tianyi Zhou, Saining Xie, Silvio Savarese, et al. Blip3-o: A family of fully open unified multimodal models-architecture, training and dataset. *arXiv preprint arXiv:2505.09568*, 2025. 2, 3
- [7] Ruidong Chen, Yancheng Bai, Xuanpu Zhang, Jianhao Zeng, Lanjun Wang, Dan Song, Lei Sun, Xiangxiang Chu, and Anan Liu. Layer-wise instance binding for regional and occlusion control in text-to-image diffusion transformers. *arXiv preprint arXiv:2603.05769*, 2026. 2
- [8] Xiangxiang Chu, Renda Li, and Yong Wang. Usp: Unified self-supervised pretraining for image generation and understanding. *arXiv preprint arXiv:2503.06132*, 2025. 13
- [9] Jia Deng, Wei Dong, Richard Socher, Li-Jia Li, Kai Li, and Li Fei-Fei. Imagenet: A large-scale hierarchical image database. In *2009 IEEE conference on computer vision and pattern recognition*, pages 248–255. Ieee, 2009. 4, 5, 6
- [10] Alexey Dosovitskiy. An image is worth 16x16 words: Transformers for image recognition at scale. *arXiv preprint arXiv:2010.11929*, 2020. 2, 8
- [11] Patrick Esser, Robin Rombach, and Bjorn Ommer. Taming transformers for high-resolution image synthesis. In *Proceedings of the IEEE/CVF conference on computer vision and pattern recognition*, pages 12873–12883, 2021. 2
- [12] Tsu-Jui Fu, Wenze Hu, Xianzhi Du, William Yang Wang, Yinfei Yang, and Zhe Gan. Guiding instruction-based image editing via multimodal large language models. *arXiv preprint arXiv:2309.17102*, 2023. 7
- [13] Yuying Ge, Sijie Zhao, Chen Li, Yixiao Ge, and Ying Shan. Seed-data-edit technical report: A hybrid dataset for instructional image editing. *arXiv preprint arXiv:2405.04007*, 2024. 4, 7
- [14] Zigang Geng, Binxin Yang, Tiankai Hang, Chen Li, Shuyang Gu, Ting Zhang, Jianmin Bao, Zheng Zhang, Houqiang Li, Han Hu, et al. Instructdiffusion: A generalist modeling interface for vision tasks. In *Proceedings of the IEEE/CVF Conference on computer vision and pattern recognition*, pages 12709–12720, 2024. 7
- [15] Jian Han, Jinlai Liu, Yi Jiang, Bin Yan, Yuqi Zhang, Zehuan Yuan, Bingyue Peng, and Xiaobing Liu. Infinity: Scaling bit-wise autoregressive modeling for high-resolution image synthesis. In *Proceedings of the Computer Vision and Pattern Recognition Conference*, pages 15733–15744, 2025. 1, 2
- [16] Haodong He, Yancheng Bai, Rui Lan, Xu Duan, Lei Sun, Xiangxiang Chu, and Gui-Song Xia. Ragsr: Regional attention guided diffusion for image super-resolution. *arXiv preprint arXiv:2508.16158*, 2025. 1
- [17] Amir Hertz, Ron Mokady, Jay Tenenbaum, Kfir Aberman, Yael Pritch, and Daniel Cohen-Or. Prompt-to-prompt image editing with cross attention control. *arXiv preprint arXiv:2208.01626*, 2022. 2
- [18] Martin Heusel, Hubert Ramsauer, Thomas Unterthiner, Bernhard Nessler, and Sepp Hochreiter. Gans trained by a two time-scale update rule converge to a local nash equilibrium. *Advances in neural information processing systems*, 30, 2017. 5
- [19] Jonathan Ho, Ajay Jain, and Pieter Abbeel. Denoising diffusion probabilistic models. *Advances in neural information processing systems*, 33:6840–6851, 2020. 1
- [20] Jonathan Ho, Ajay Jain, and Pieter Abbeel. Denoising diffusion probabilistic models. *Advances in neural information processing systems*, 33:6840–6851, 2020. 2
- [21] Xuan Ju, Ailing Zeng, Yuxuan Bian, Shaoteng Liu, and Qiang Xu. Pnp inversion: Boosting diffusion-based editing with 3 lines of code. *International Conference on Learning Representations (ICLR)*, 2024. 5, 6, 7
- [22] Diederik P Kingma, Max Welling, et al. Auto-encoding variational bayes, 2013. 2
- [23] Alexander Kirillov, Eric Mintun, Nikhila Ravi, Hanzi Mao, Chloe Rolland, Laura Gustafson, Tete Xiao, Spencer Whitehead, Alexander C Berg, Wan-Yen Lo, et al. Segment anything. In *Proceedings of the IEEE/CVF international conference on computer vision*, pages 4015–4026, 2023. 8
- [24] Rui Lan, Yancheng Bai, Xu Duan, Mingxing Li, Dongyang Jin, Ryan Xu, Lei Sun, and Xiangxiang Chu. Flux-text: A simple and advanced diffusion transformer baseline for scene text editing. *arXiv preprint arXiv:2505.03329*, 2025. 1, 2
- [25] Haopeng Li, Jinyue Yang, Kexin Wang, Xuerui Qiu, Yuhong Chou, Xin Li, and Guoqi Li. Scalable autoregressive image generation with mamba. *arXiv preprint arXiv:2408.12245*, 2024. 2, 3
- [26] Han Li, Xinyu Peng, Yaoming Wang, Zelin Peng, Xin Chen, Rongxiang Weng, Jingang Wang, Xunliang Cai, Wenrui Dai, and Hongkai Xiong. Onecat: Decoder-only auto-regressive model for unified understanding and generation. *arXiv preprint arXiv:2509.03498*, 2025. 1
- [27] Ming Li, Taojiannan Yang, Huafeng Kuang, Jie Wu, Zhaoning Wang, Xuefeng Xiao, and Chen Chen. Controlnet++: Improving conditional controls with efficient consistency feedback. *arXiv preprint arXiv:2404.07987*, 2024. 1

- [28] Ming Li, Taojiannan Yang, Huafeng Kuang, Jie Wu, Zhaoning Wang, Xuefeng Xiao, and Chen Chen. Controlnet++: Improving conditional controls with efficient consistency feedback. In *European Conference on Computer Vision*, pages 129–147. Springer, 2024. 6, 7
- [29] Tianhong Li, Dina Katabi, and Kaiming He. Return of unconditional generation: A self-supervised representation generation method. *Advances in Neural Information Processing Systems*, 37:125441–125468, 2024. 13
- [30] Xiang Li, Kai Qiu, Hao Chen, Jason Kuen, Zhe Lin, Rita Singh, and Bhiksha Raj. Controlvar: Exploring controllable visual autoregressive modeling. *arXiv preprint arXiv:2406.09750*, 2024. 3, 5, 6
- [31] Yuheng Li, Haotian Liu, Qingyang Wu, Fangzhou Mu, Jianwei Yang, Jianfeng Gao, Chunyuan Li, and Yong Jae Lee. Gligen: Open-set grounded text-to-image generation. In *Proceedings of the IEEE/CVF conference on computer vision and pattern recognition*, pages 22511–22521, 2023. 6, 7
- [32] Zongming Li, Tianheng Cheng, Shoufa Chen, Peize Sun, Haocheng Shen, Longjin Ran, Xiaoxin Chen, Wenyu Liu, and Xinggang Wang. Controlar: Controllable image generation with autoregressive models. *arXiv preprint arXiv:2410.02705*, 2024. 1, 3, 5, 6, 7, 8, 13, 15
- [33] Weifeng Lin, Xinyu Wei, Ruichuan An, Peng Gao, Bocheng Zou, Yulin Luo, Siyuan Huang, Shanghang Zhang, and Hongsheng Li. Draw-and-understand: Leveraging visual prompts to enable mllms to comprehend what you want. *arXiv preprint arXiv:2403.20271*, 2024. 13
- [34] Weifeng Lin, Xinyu Wei, Ruichuan An, Tianhe Ren, Tingwei Chen, Renrui Zhang, Ziyu Guo, Wentao Zhang, Lei Zhang, and Hongsheng Li. Perceive anything: Recognize, explain, caption, and segment anything in images and videos, 2025. 13
- [35] Dongyang Liu, Shitian Zhao, Le Zhuo, Weifeng Lin, Yu Qiao, Hongsheng Li, and Peng Gao. Lumina-mgpt: Illuminate flexible photorealistic text-to-image generation with multimodal generative pretraining. *arXiv preprint arXiv:2408.02657*, 2024. 1, 3
- [36] Jinlai Liu, Jian Han, Bin Yan, Hui Wu, Fengda Zhu, Xing Wang, Yi Jiang, Bingyue Peng, and Zehuan Yuan. Infinitystar: Unified spacetime autoregressive modeling for visual generation. *arXiv preprint arXiv:2511.04675*, 2025. 1
- [37] Keli Liu, Zhendong Wang, Wengang Zhou, Shaodong Xu, Ruixiao Dong, and Houqiang Li. Scaleweaver: Weaving efficient controllable t2i generation with multi-scale reference attention. *arXiv preprint arXiv:2510.14882*, 2025. 13
- [38] Yulin Luo, Ruichuan An, Bocheng Zou, Yiming Tang, Jiaming Liu, and Shanghang Zhang. Llm as dataset analyst: Subpopulation structure discovery with large language model. In *European Conference on Computer Vision*, pages 235–252. Springer, 2024. 13
- [39] Zhuoyan Luo, Fengyuan Shi, Yixiao Ge, Yujiu Yang, Limin Wang, and Ying Shan. Open-magvit2: An open-source project toward democratizing auto-regressive visual generation. *arXiv preprint arXiv:2409.04410*, 2024. 2
- [40] Chuofan Ma, Yi Jiang, Junfeng Wu, Jihan Yang, Xin Yu, Zehuan Yuan, Bingyue Peng, and Xiaojuan Qi. Unitok: A unified tokenizer for visual generation and understanding. *arXiv preprint arXiv:2502.20321*, 2025. 2, 3
- [41] Jingzhe Ma, Haoyu Luo, Zixu Huang, Dongyang Jin, Rui Wang, Johann A Briffa, Norman Poh, and Shiqi Yu. Passersby-anonymizer: Safeguard the privacy of passersby in social videos. In *2024 IEEE International Joint Conference on Biometrics (IJCB)*, pages 1–10. IEEE, 2024. 2
- [42] Xiaoxiao Ma, Mohan Zhou, Tao Liang, Yalong Bai, Tiejun Zhao, Huaian Chen, and Yi Jin. Star: Scale-wise text-to-image generation via auto-regressive representations. *arXiv preprint arXiv:2406.10797*, 2024. 2
- [43] Xiaoxiao Ma, Haibo Qiu, Guohui Zhang, Zhixiong Zeng, Siqi Yang, Lin Ma, and Feng Zhao. Stage: Stable and generalizable grpo for autoregressive image generation. *arXiv preprint arXiv:2509.25027*, 2025. 2
- [44] Xu Ma, Peize Sun, Haoyu Ma, Hao Tang, Chih-Yao Ma, Jialiang Wang, Kunpeng Li, Xiaoliang Dai, Yujun Shi, Xuan Ju, et al. Token-shuffle: Towards high-resolution image generation with autoregressive models. *arXiv preprint arXiv:2504.17789*, 2025. 4
- [45] Xiaoxiao Ma, Feng Zhao, Pengyang Ling, Haibo Qiu, Zhixiang Wei, Hu Yu, Jie Huang, Zhixiong Zeng, and Lin Ma. Towards better & faster autoregressive image generation: From the perspective of entropy. *arXiv preprint arXiv:2510.09012*, 2025. 2
- [46] Chenlin Meng, Yutong He, Yang Song, Jiaming Song, Jiajun Wu, Jun-Yan Zhu, and Stefano Ermon. Sdedit: Guided image synthesis and editing with stochastic differential equations. *arXiv preprint arXiv:2108.01073*, 2021. 1, 2
- [47] Mehdi Mirza and Simon Osindero. Conditional generative adversarial nets. *arXiv preprint arXiv:1411.1784*, 2014. 2
- [48] Chong Mou, Xintao Wang, Liangbin Xie, Yanze Wu, Jian Zhang, Zhongang Qi, and Ying Shan. T2i-adapter: Learning adapters to dig out more controllable ability for text-to-image diffusion models. In *Proceedings of the AAAI conference on artificial intelligence*, pages 4296–4304, 2024. 5, 6
- [49] Chong Mou, Xintao Wang, Liangbin Xie, Yanze Wu, Jian Zhang, Zhongang Qi, and Ying Shan. T2i-adapter: Learning adapters to dig out more controllable ability for text-to-image diffusion models. In *Proceedings of the AAAI Conference on Artificial Intelligence*, pages 4296–4304, 2024. 2, 7
- [50] Jiteng Mu, Nuno Vasconcelos, and Xiaolong Wang. Editar: Unified conditional generation with autoregressive models. In *Proceedings of the Computer Vision and Pattern Recognition Conference*, pages 7899–7909, 2025. 1, 2, 3, 6, 7, 13, 15
- [51] Alexander Quinn Nichol and Prafulla Dhariwal. Improved denoising diffusion probabilistic models. In *International Conference on Machine Learning*, pages 8162–8171, 2021. 2
- [52] Maxime Oquab, Timothée Darcet, Théo Moutakanni, Huy Vo, Marc Szafraniec, Vasil Khalidov, Pierre Fernandez, Daniel Haziza, Francisco Massa, Alaaeldin El-Nouby, et al. Dinov2: Learning robust visual features without supervision. *arXiv preprint arXiv:2304.07193*, 2023. 2, 3, 4, 8, 13
- [53] William Peebles and Saining Xie. Scalable diffusion models with transformers. In *Proceedings of the IEEE/CVF Inter-*

- national Conference on Computer Vision*, pages 4195–4205, 2023. 1, 2
- [54] Long Peng, Yang Cao, Renjing Pei, Wenbo Li, Jiaming Guo, Xueyang Fu, Yang Wang, and Zheng-Jun Zha. Efficient real-world image super-resolution via adaptive directional gradient convolution. *arXiv preprint arXiv:2405.07023*, 2024. 13
- [55] Pablo Pernias, Dominic Rampas, Mats L Richter, Christopher J Pal, and Marc Aubreville. Würstchen: An efficient architecture for large-scale text-to-image diffusion models. *arXiv preprint arXiv:2306.00637*, 2023. 13
- [56] Dustin Podell, Zion English, Kyle Lacey, Andreas Blattmann, Tim Dockhorn, Jonas Müller, Joe Penna, and Robin Rombach. Sdxl: Improving latent diffusion models for high-resolution image synthesis. *arXiv preprint arXiv:2307.01952*, 2023. 1
- [57] Can Qin, Shu Zhang, Ning Yu, Yihao Feng, Xinyi Yang, Yingbo Zhou, Huan Wang, Juan Carlos Niebles, Caiming Xiong, Silvio Savarese, et al. Unicontrol: A unified diffusion model for controllable visual generation in the wild. *arXiv preprint arXiv:2305.11147*, 2023. 6
- [58] Can Qin, Shu Zhang, Ning Yu, Yihao Feng, Xinyi Yang, Yingbo Zhou, Huan Wang, Juan Carlos Niebles, Caiming Xiong, Silvio Savarese, et al. Unicontrol: A unified diffusion model for controllable visual generation in the wild. *arXiv preprint arXiv:2305.11147*, 2023. 1, 2, 4, 5, 6, 7, 8, 13
- [59] Xiangyan Qu, Zhenlong Yuan, Jing Tang, Rui Chen, Datao Tang, Meng Yu, Lei Sun, Yancheng Bai, Xiangxiang Chu, Gaopeng Gou, et al. From scale to speed: Adaptive test-time scaling for image editing. *arXiv preprint arXiv:2603.00141*, 2026. 2
- [60] Yunpeng Qu, Kun Yuan, Jinhua Hao, Kai Zhao, Qizhi Xie, Ming Sun, and Chao Zhou. Visual autoregressive modeling for image super-resolution. *arXiv preprint arXiv:2501.18993*, 2025. 3
- [61] Alec Radford, Jong Wook Kim, Chris Hallacy, Aditya Ramesh, Gabriel Goh, Sandhini Agarwal, Girish Sastry, Amanda Askell, Pamela Mishkin, Jack Clark, et al. Learning transferable visual models from natural language supervision. In *International conference on machine learning*, pages 8748–8763. PMLR, 2021. 2, 8
- [62] Colin Raffel, Noam Shazeer, Adam Roberts, Katherine Lee, Sharan Narang, Michael Matena, Yanqi Zhou, Wei Li, and Peter J Liu. Exploring the limits of transfer learning with a unified text-to-text transformer. *Journal of machine learning research*, 21(140):1–67, 2020. 2, 5
- [63] Jingjing Ren, Wenbo Li, Haoyu Chen, Renjing Pei, Bin Shao, Yong Guo, Long Peng, Fenglong Song, and Lei Zhu. Ultrapixel: Advancing ultra high-resolution image synthesis to new peaks. *Advances in Neural Information Processing Systems*, 37:111131–111171, 2024. 13
- [64] Robin Rombach, Andreas Blattmann, Dominik Lorenz, Patrick Esser, and Björn Ommer. High-resolution image synthesis with latent diffusion models. *Proceedings of the IEEE/CVF Conference on Computer Vision and Pattern Recognition*, pages 10684–10695, 2022. 2
- [65] Chitwan Saharia, William Chan, Saurabh Saxena, Lala Li, Jay Whang, Emily L Denton, Kamyar Ghasemipour, Raphael Gontijo Lopes, Burcu Karagol Ayan, Tim Salimans, et al. Photorealistic text-to-image diffusion models with deep language understanding. *Advances in neural information processing systems*, 35:36479–36494, 2022. 2
- [66] Wenzhe Shi, Jose Caballero, Ferenc Huszár, Johannes Totz, Andrew P Aitken, Rob Bishop, Daniel Rueckert, and Zehan Wang. Real-time single image and video super-resolution using an efficient sub-pixel convolutional neural network. In *Proceedings of the IEEE conference on computer vision and pattern recognition*, pages 1874–1883, 2016. 4
- [67] Uriel Singer, Adam Polyak, Thomas Hayes, Xi Yin, Jie An, Songyang Zhang, Qiyuan Hu, Harry Yang, Oron Ashual, Oran Gafni, et al. Make-a-video: Text-to-video generation without text-video data. *arXiv preprint arXiv:2209.14792*, 2022. 2
- [68] Dan Song, Jian-Hao Zeng, Min Liu, Xuan-Ya Li, and An-An Liu. Fashion customization: Image generation based on editing clue. *IEEE Transactions on Circuits and Systems for Video Technology*, 34(6):4434–4444, 2023. 2
- [69] Peize Sun, Yi Jiang, Shoufa Chen, Shilong Zhang, Bingyue Peng, Ping Luo, and Zehuan Yuan. Autoregressive model beats diffusion: Llama for scalable image generation. *arXiv preprint arXiv:2406.06525*, 2024. 1, 2, 3, 5, 15
- [70] Haotian Tang, Yecheng Wu, Shang Yang, Enze Xie, Junsong Chen, Junyu Chen, Zhuoyang Zhang, Han Cai, Yao Lu, and Song Han. Hart: Efficient visual generation with hybrid autoregressive transformer. *arXiv preprint arXiv:2410.10812*, 2024. 2
- [71] Keyu Tian, Yi Jiang, Zehuan Yuan, Bingyue Peng, and Liwei Wang. Visual autoregressive modeling: Scalable image generation via next-scale prediction. *arXiv preprint arXiv:2404.02905*, 2024. 1, 2, 3, 5
- [72] Hugo Touvron, Thibaut Lavril, Gautier Izacard, Xavier Martinet, Marie-Anne Lachaux, Timothée Lacroix, Baptiste Rozière, Naman Goyal, Eric Hambro, Faisal Azhar, et al. Llama: Open and efficient foundation language models. *arXiv preprint arXiv:2302.13971*, 2023. 2, 3
- [73] Aaron Van Den Oord, Nal Kalchbrenner, and Koray Kavukcuoglu. Pixel recurrent neural networks. In *International conference on machine learning*, pages 1747–1756. PMLR, 2016. 2
- [74] Aaron Van Den Oord, Oriol Vinyals, et al. Neural discrete representation learning. *Advances in neural information processing systems*, 30, 2017. 2, 3
- [75] Jiyuan Wang, Chunyu Lin, Lang Nie, Kang Liao, Shuwei Shao, and Yao Zhao. Digging into contrastive learning for robust depth estimation with diffusion models. In *Proceedings of the 32nd ACM International Conference on Multimedia*, page 4129–4137. ACM, 2024. 2
- [76] Jiyuan Wang, Chunyu Lin, Cheng Guan, Lang Nie, Jing He, Haodong Li, Kang Liao, and Yao Zhao. Jasmine: Harnessing diffusion prior for self-supervised depth estimation. *arXiv preprint arXiv:2503.15905*, 2025. 2
- [77] JiYuan Wang, Chunyu Lin, Lei Sun, Rongying Liu, Lang Nie, Mingxing Li, Kang Liao, Xiangxiang Chu, and Yao Zhao. From editor to dense geometry estimator. *arXiv preprint arXiv:2509.04338*, 2025. 2

- [78] Zhixiang Wei, Guangting Wang, Xiaoxiao Ma, Ke Mei, Huaian Chen, Yi Jin, and Fengyun Rao. Hq-clip: Leveraging large vision-language models to create high-quality image-text datasets and clip models. In *Proceedings of the IEEE/CVF International Conference on Computer Vision*, pages 22447–22456, 2025. 2
- [79] Ge Wu, Shen Zhang, Ruijing Shi, Shanghua Gao, Zhenyuan Chen, Lei Wang, Zhaowei Chen, Hongcheng Gao, Yao Tang, Jian Yang, et al. Representation entanglement for generation: Training diffusion transformers is much easier than you think. *arXiv preprint arXiv:2507.01467*, 2025. 13
- [80] Size Wu, Wenwei Zhang, Lumin Xu, Sheng Jin, Zhonghua Wu, Qingyi Tao, Wentao Liu, Wei Li, and Chen Change Loy. Harmonizing visual representations for unified multimodal understanding and generation. *arXiv preprint arXiv:2503.21979*, 2025. 2, 3
- [81] Yi Xin, Juncheng Yan, Qi Qin, Zhen Li, Dongyang Liu, Shicheng Li, Victor Shea-Jay Huang, Yupeng Zhou, Renrui Zhang, Le Zhuo, et al. Lumina-mgpt 2.0: Stand-alone autoregressive image modeling. *arXiv preprint arXiv:2507.17801*, 2025. 1, 3
- [82] Hao Xu, Long Peng, Shezheng Song, Xiaodong Liu, Ma Jun, Shasha Li, Jie Yu, and Xiaoguang Mao. Camel: Energy-aware llm inference on resource-constrained devices. *arXiv preprint arXiv:2508.09173*, 2025. 13
- [83] Ryan Xu, Dongyang Jin, Yancheng Bai, Rui Lan, Xu Duan, Lei Sun, and Xiangxiang Chu. Scalar: Scale-wise controllable visual autoregressive learning. *arXiv preprint arXiv:2507.19946*, 2025. 3, 13
- [84] Jingfeng Yao, Bin Yang, and Xinggang Wang. Reconstruction vs. generation: Taming optimization dilemma in latent diffusion models. In *Proceedings of the Computer Vision and Pattern Recognition Conference*, pages 15703–15712, 2025. 13
- [85] Ziyu Yao, Jialin Li, Yifeng Zhou, Yong Liu, Xi Jiang, Chengjie Wang, Feng Zheng, Yuexian Zou, and Lei Li. Car: Controllable autoregressive modeling for visual generation. *arXiv preprint arXiv:2410.04671*, 2024. 3, 5, 6, 8, 13
- [86] Sihyun Yu, Sangkyung Kwak, Huiwon Jang, Jongheon Jeong, Jonathan Huang, Jinwoo Shin, and Saining Xie. Representation alignment for generation: Training diffusion transformers is easier than you think. In *The Thirteenth International Conference on Learning Representations*. 13
- [87] Jianhao Zeng, Dan Song, Weizhi Nie, Hongshuo Tian, Tongtong Wang, and An-An Liu. Cat-dm: Controllable accelerated virtual try-on with diffusion model. In *Proceedings of the IEEE/CVF conference on computer vision and pattern recognition*, pages 8372–8382, 2024. 2
- [88] Jianhao Zeng, Yancheng Bai, Ruidong Chen, Xuanpu Zhang, Lei Sun, Dongyang Jin, Ryan Xu, Nannan Zhang, Dan Song, and Xiangxiang Chu. Eevee: Towards close-up high-resolution video-based virtual try-on. *arXiv preprint arXiv:2511.18957*, 2025. 2
- [89] Lvmin Zhang, Anyi Rao, and Maneesh Agrawala. Adding conditional control to text-to-image diffusion models. In *Proceedings of the IEEE/CVF International Conference on Computer Vision*, pages 3836–3847, 2023. 1, 2
- [90] Lvmin Zhang, Anyi Rao, and Maneesh Agrawala. Adding conditional control to text-to-image diffusion models. In *Proceedings of the IEEE/CVF international conference on computer vision*, pages 3836–3847, 2023. 5, 6, 7
- [91] Nannan Zhang, Yijiang Li, Dong Du, Zheng Chong, Zhengwentai Sun, Jianhao Zeng, Yusheng Dai, Zhengyu Xie, Hairui Zhu, and Xiaoguang Han. Robust-mvton: Learning cross-pose feature alignment and fusion for robust multi-view virtual try-on. In *Proceedings of the Computer Vision and Pattern Recognition Conference*, pages 16029–16039, 2025. 2
- [92] Xuanpu Zhang, Dan Song, Pengxin Zhan, Tianyu Chang, Jianhao Zeng, Qingguo Chen, Weihua Luo, and An-An Liu. Boow-vton: Boosting in-the-wild virtual try-on via mask-free pseudo data training. In *Proceedings of the Computer Vision and Pattern Recognition Conference*, pages 26399–26408, 2025. 2
- [93] Shihao Zhao, Dongdong Chen, Yen-Chun Chen, Jianmin Bao, Shaozhe Hao, Lu Yuan, and Kwan-Yee K Wong. Uni-controlnet: All-in-one control to text-to-image diffusion models. *Advances in Neural Information Processing Systems*, 36:11127–11150, 2023. 6
- [94] Shihao Zhao, Dongdong Chen, Yen-Chun Chen, Jianmin Bao, Shaozhe Hao, Lu Yuan, and Kwan-Yee K Wong. Uni-controlnet: All-in-one control to text-to-image diffusion models. *Advances in Neural Information Processing Systems*, 36, 2024. 7
- [95] Hongkai Zheng, Weili Nie, Arash Vahdat, and Anima Anandkumar. Fast training of diffusion models with masked transformers. *arXiv preprint arXiv:2306.09305*, 2023. 13
- [96] Xianwei Zhuang, Yuxin Xie, Yufan Deng, Liming Liang, Jinghan Ru, Yuguo Yin, and Yuexian Zou. Vargpt: Unified understanding and generation in a visual autoregressive multimodal large language model, 2025. 1, 2, 3

## A. More Discussion

### Decoding-stage Injection vs. Prefilling-stage condition.

Conditioning strategies for autoregressive (AR) models fall into two categories: decoding-stage injection and prefilling-stage conditioning. We argue that the latter provides a more suitable conditioning mechanism for instruction editing and controllable generation, while remaining naturally compatible with both next-token and next-set AR paradigms.

For controllable generation, decoding-stage methods [32, 37, 83, 85] like ControlAR [32] and CAR [85] inject control signals into intermediate layers, enabling fine-grained spatial alignment. However, this tight coupling often leads to training instability and overfitting to local structures, resulting in blurry textures and reduced realism. In contrast, prefilling-based methods such as EditAR [50] and our SCAR prepend control features as conditioning tokens before decoding. Though offering slightly weaker pixel-level control, this design leads to sharper, more natural outputs and better generalization across control types. More importantly, for instruction editing, decoding-stage injection fails to align generation with high-level semantics, often producing overconstrained or inconsistent results. It also conflicts with unified multimodal models (UMM) [2, 3, 33, 34, 38, 54, 63, 82], as spatial injection disrupts the shared AR generation. Prefilling-stage conditioning avoids this issue, integrates cleanly with UMM, and better preserves semantic intent during generation.

**Semantic Prefix vs. VQ Prefix.** Table 7 reports the quantitative comparison between semantically aligned DINO tokens and standard VQ tokens under two compression settings ( $k^2=1\times$  and  $4\times$ ) on MultiGen-20M [58]. Across both settings, DINO tokens consistently outperform VQ tokens, underscoring the effectiveness of our semantic prefix for autoregressive editing. Without the compression ( $1\times$  compression) setting, DINO tokens improve SSIM by +1.96 and reduce FID by 0.91, indicating better perceptual quality and semantic coherence. Under the  $4\times$  compression setting, the improvement becomes even more pronounced: SSIM increases by +3.21, and FID drops by 2.83. These results demonstrate that our method not only improves generation quality in standard setups but also maintains strong performance under token compression.

**Discussion on Semantic Alignment.** Recent work increasingly suggests that enforcing semantic representation alignment can lead to more effective learning in generative models. In diffusion models, REPA [86] aligns internal features with pretrained semantic encoders to stabilize training and improve generation. REG [79] takes a different path by injecting discriminative semantics directly via spatial concatenation with a class token, improving quality and convergence with minimal overhead. VA-VAE [84] enhances latent interpretability via representation alignment in VAEs. MaskDiT [95] enforces semantic

Table 7. Comparison between the semantical DINO token and the VQ token under different compression ratios. All models are trained for 1 epoch. Values in parentheses indicate relative improvement over VQ tokens.

Prefix Condition	Compress Ratio $k^2$	HED	
		FID↓	SSIM↑
VQ token	$1\times$	10.20	79.99
DINO token	$1\times$	9.29 (-0.91)	81.95 (+1.96)
VQ token	$4\times$	12.26	78.55
DINO token	$4\times$	9.43 (-2.83)	81.76 (+3.21)

consistency through masked reconstruction or auxiliary decoders. Multi-stage methods [29, 55] leverage pretrained representations as intermediate maps, while USP [8] aligns masked latents in a shared VAE space to unify generation and understanding.

While these strategies have shown strong results in diffusion-based models, extending semantic alignment to autoregressive (AR) frameworks for editing presents unique challenges. EditAR [50] attempts this by distilling supervision from DINO features onto the hidden states of generated VQ tokens. However, as this supervision is applied post-generation, it lacks explicit semantic flow during decoding.

In contrast, SCAR aligns semantic features at the prefilling stage, by matching conditional representations from the source image with a pretrained visual space (e.g., DINO [52]) before decoding begins. This design fits naturally with the AR model’s causal structure, introducing dense supervision without interfering with token-level predictions. As a result, the model internalizes the semantic correspondence early and propagates it consistently throughout generation. Compared to global alignment strategies in diffusion or post-hoc distillation in EditAR, SCAR provides a more direct and effective mechanism for integrating conditional guidance, especially in instruction-based editing where semantic consistency across text, condition, and output is critical.

## B. More Visualization

### B.1. About Semantic Alignment Guidance

As shown in Figure 8, without Semantic Alignment Guidance, the model may sometimes produce incomplete or ambiguous edits. Semantic Alignment Guidance mitigates this by strengthening the correspondence between input conditions and target semantics. In the apple relocation example (top row), both the *w/o*  $\mathcal{L}_{\text{align}}$  and  $\delta=0.3$  results retain table textures, indicating insufficient background change. In contrast,  $\delta=0.5$  successfully introduces grass while preserving the foreground. However,  $\delta=1.0$  causes a global green tint, suggesting semantic leakage. In the background editing task (middle row),  $\delta=1.0$  enhances the rainy effect but removes fine details such as leaves, while  $\delta=0.5$  better bal-

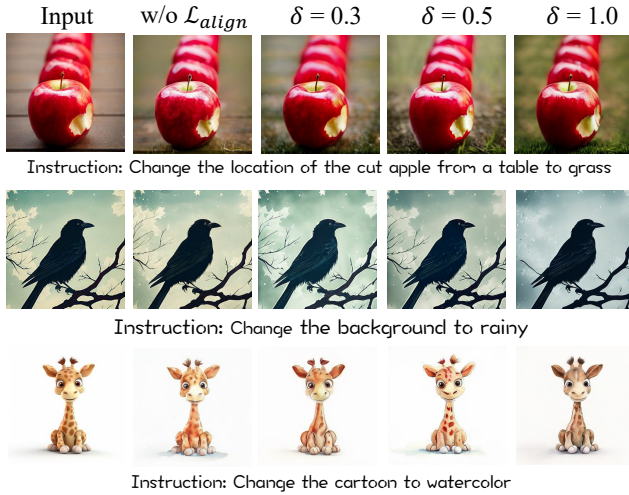


Figure 8. Additional visualizations on Semantic Alignment Guidance  $\mathcal{L}_{align}$  in Equation (8).

ances visual accuracy and structure. For stylization (bottom row), larger  $\delta$  values improve the watercolor effect, but  $\delta=1.0$  leads to facial distortion and oversaturation.

Overall, moderate alignment strength improves consistency and visual quality, whereas excessive supervision may cause artifacts or semantic drift.

## B.2. Instruction Editing

As shown in Figure 9, we present additional visualizations for instruction editing, further demonstrating the effectiveness of our proposed SCAR.

## B.3. Controllable Generation

**C2I Controllable Generation by SCAR-Uni.** In C2I Controllable Generation, we focus on the results of SCAR-Uni, a unified method that supports diverse control conditions using the same model. As shown in Figure 10, SCAR-Uni generates high-quality images while maintaining strong controllability across diverse input types.

**T2I Controllable Generation.** Figure 11 presents additional visualizations for T2I controllable generation. The results further demonstrate the strong performance and generalization ability of our proposed SCAR.

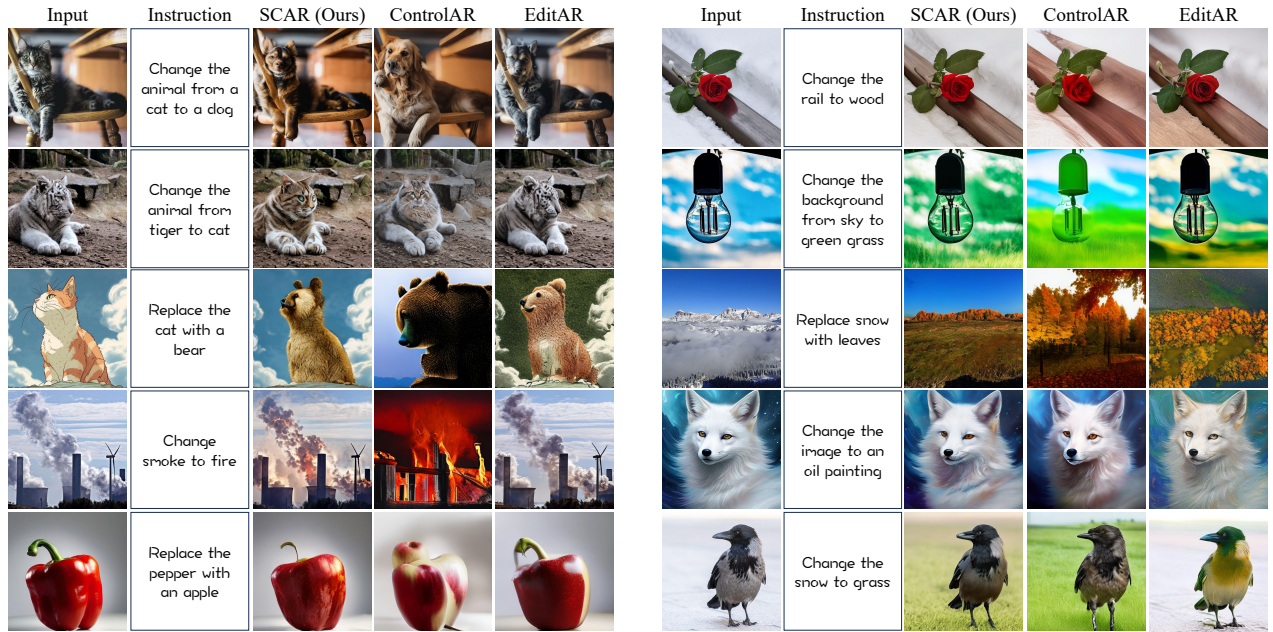


Figure 9. Additional visualizations of instruction editing results. SCAR (Ours) produces more faithful and semantically consistent edits than ControlAR [32] and EditAR [50], with all methods using the same LlamaGen-XL [69]. All visualizations are generated at a resolution of  $512 \times 512$ .

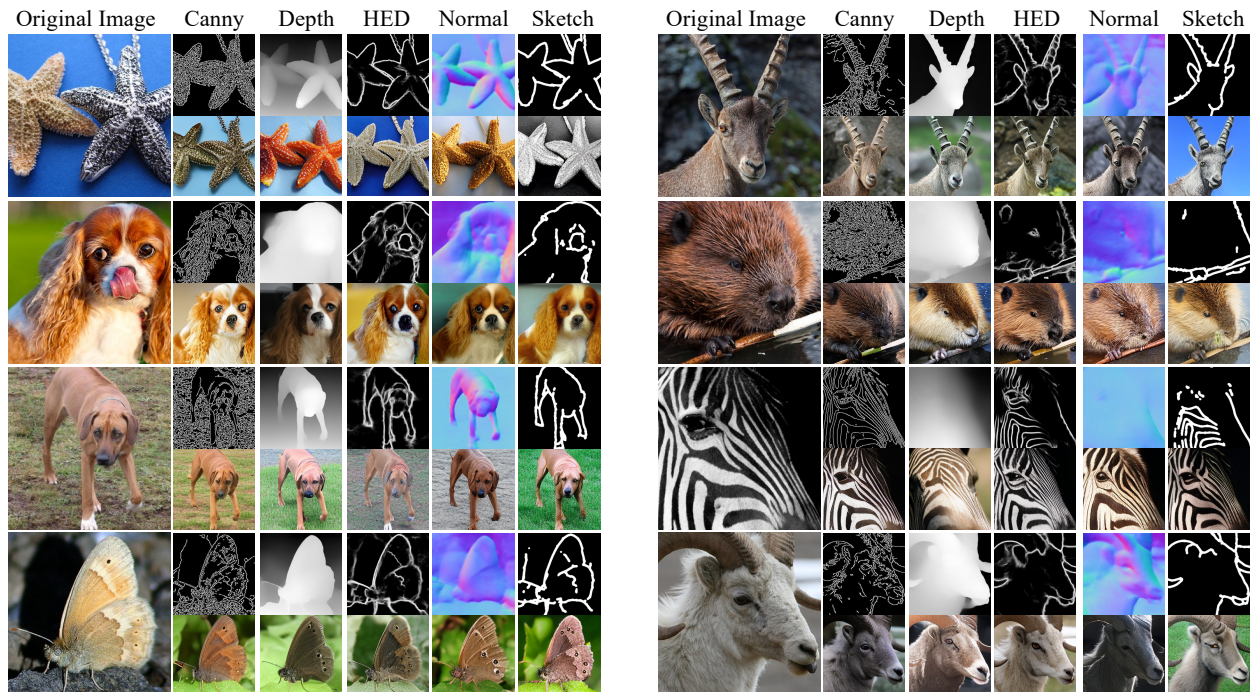


Figure 10. Additional visualizations of C2I Controllable Generation by SCAR-Uni based on LlamaGen-L. We adopt five different control conditions: Canny, Depth, HED, Normal, and Sketch. All visualizations are generated at a resolution of  $256 \times 256$ .

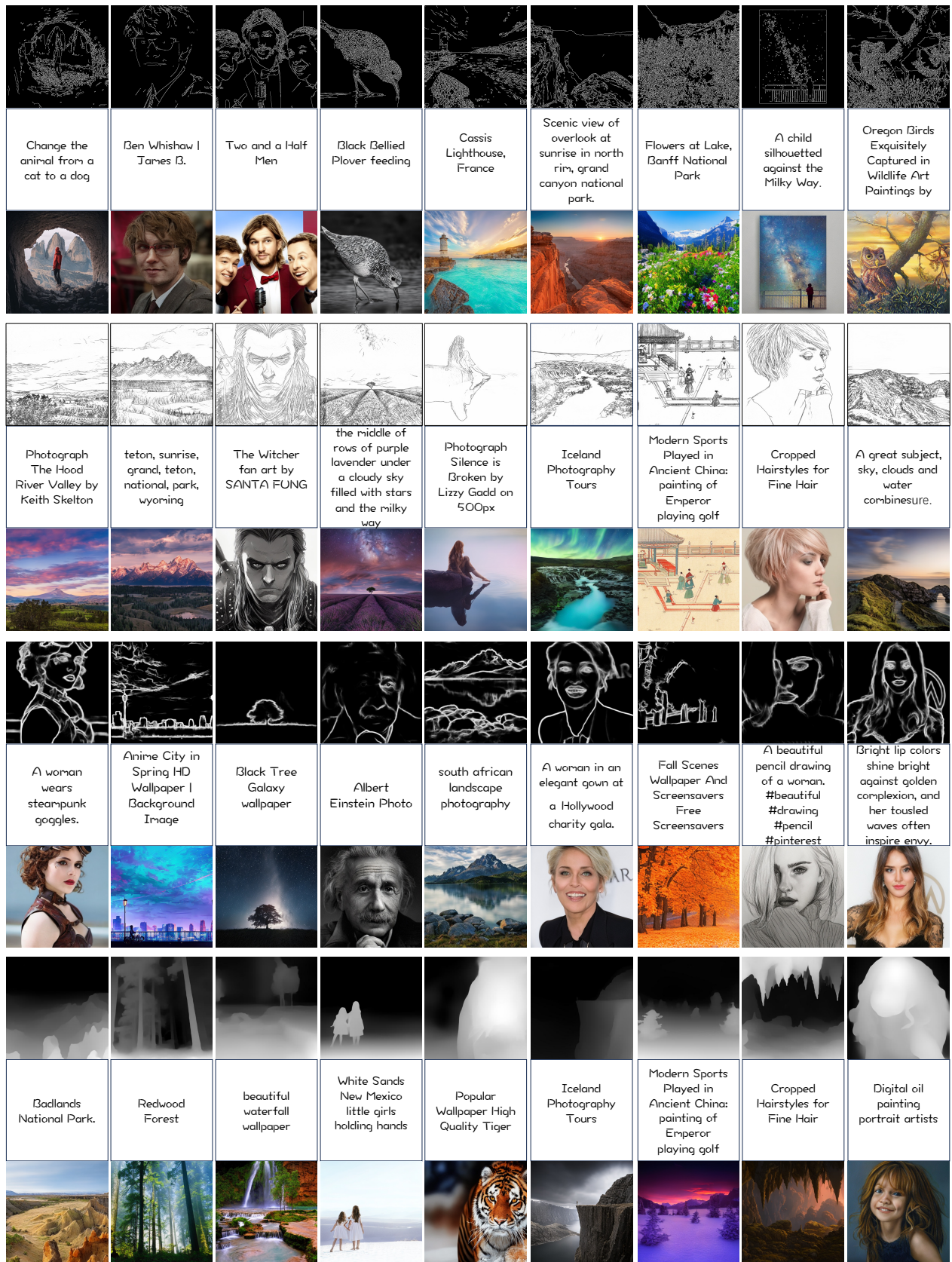


Figure 11. Additional visualizations of T2I Controllable Generation by SCAR based on LlamaGen-XL. To demonstrate the controllability and generalization ability of our SCAR, we present results under four control conditions: Canny, Depth, HED, and Lineart. All images are generated at a resolution of 512x512.